

Constrained Particle Filtering for Movement Identification in Forearm Prosthesis

Nesrine Amor^{a,*}, Ghulam Rasool^b, Nidhal C. Bouaynaya^b,
Roman Shterenberg^c

^a*National Superior School of Engineers of Tunis (ENSIT), University of Tunis, Tunisia*

^b*Department of Electrical and Computer Engineering, Rowan University, 201 Mullica Hill Road, Glassboro, New Jersey, USA*

^c*Department of Mathematics, University of Alabama at Birmingham, Birmingham, AL, USA*

Abstract

We formulate the problem of movement identification for the forearm prosthesis using a nonlinear state-space system and the hypothesis of muscle synergies. The synergy activation coefficients contain task-specific information and can be used to identify limb movements. In the proposed framework, the measurements are EMG data and the system state consists of muscle synergy activation coefficients, which are physiologically constrained to be nonnegative on average. Particle filters are the state-of-the-art techniques for optimal state estimation in nonlinear and non-Gaussian systems. However, the very numerical nature of the particle filters, which constitutes their strength, becomes their major weakness in handling constraints on the state. In this paper, we solve the movement identification problem by introducing a constrained particle filter termed as mean density truncation (MiND). We show that MiND minimally perturbs the unconstrained distribution of the state while simultaneously satisfying the desired constraints on the unknown state. We recorded EMG data from forearm muscles of 12 participants for identification of hand and wrist movements. The proposed particle filtering with MiND provided an accurate stream of synergy activation coefficients ($p < 0.001$) which were used for movement identification with error rates significantly lower ($p < 0.05$) than currently used heuristics and Linear Discriminate Analysis.

Keywords: Constrained particle filter, electromyogram, muscle synergy, prosthesis.

*Corresponding author

Email address: nisrine.amor@hotmail.fr (Nesrine Amor)

1. Introduction

Electromyogram (EMG) provides an insight into the neural processes taking place in the central nervous system (CNS) for planning and execution of voluntary tasks [1–4]. Clinicians and researchers have used EMG signals for 5 studying muscle functions and related neural processes in healthy as well as pathological conditions [1, 5–8]. Recently, due to advances in machine learning techniques, surface EMG signals have been widely used for movement identification and control of powered prosthetic devices in individuals with acquired or congenital amputations [9–12]. The surface EMG signals recorded from the 10 leftover muscles are initially used to train a supervised or unsupervised machine learning algorithm. Later, based on the EMG signals recorded from the same muscles, the algorithm identifies the performed movement [9, 13]. Although machine learning algorithms provide classification accuracy numbers in the range of 90% or above for movement identification [13], clinical applications and user 15 acceptance of this technology are still limited [14–16].

One reason for this shortcoming is that machine learning algorithms may not take into account valuable information about system physiology and underlying dynamics [15, 17]. In particular, the crucial information about the hidden neural processes that generate observable (through EMG signals) muscle activation 20 patterns cannot be explicitly incorporated into machine learning algorithms. In contrast, physiologically relevant mathematical models for movement identification, that incorporate all available information about the system physiology and underlying neural processes, can be built using the state-space framework [17, 18].

Muscle synergies are hypothesized as building blocks that the CNS can combine to generate complex behaviors [19, 20]. By definition, muscle synergies are 25 task-specific relative fixed levels of muscle activations that the CNS can activate, using fewer commands, to generate purposeful behavior. Muscle synergies may be considered a solution to the degrees-of-freedom (DOF) problem in the motor 30 control arising due to the presence of a large number of muscles as compared to the number of joints [21, 22]. Whether the CNS uses muscle synergies to control muscles or whether the muscle synergies have a neural origin or not are still open research questions [21, 23]. However, the hypothesis of muscle synergies provides a plausible computational framework for understanding and modeling 35 functions of the CNS [17, 24, 25].

Recently, Rasool et al. proposed a linear state-space model for movement 40 identification [17]. The Kalman filter was used to estimate the state which was then projected onto the nonnegative region. However, it is argued that the synergy coefficients represent a low-dimensional encoding of task-specific muscle activations that evolve nonlinearly due to the thresholding actions of individual motor neurons, transportation delays in neural signal processing, and related nonlinear biochemical processes [26]. Thus, a nonlinear state-space system is warranted to model the behavior of nonnegative synergy activation coefficients 45 accurately for movement identification. As a result, we are confronted with a nonlinear and constrained estimation problem.

Particle filters solve the optimal estimation problem in nonlinear and non-Gaussian scenarios by approximating the state posterior probability density function using a set of weighted particles [27]. The density approximation by the particle filter converges, in the mean squared error and under mild conditions, 50 to the actual posterior density function of the unknown state [28]. However, there is no optimal framework for incorporating constraints enforced on the latent system state in particle filters. Systematic efforts to integrate constraints imposed on the state in particle filters framework are limited and heuristic in nature [29–32].

55 A widely used approach is acceptance/rejection scheme, which enforces the constraint by simply rejecting all particles violating the constraint [29, 33]. However, except for the case when an appropriate and almost perfect proposal density function is available, the number of rejected particles may increase quickly, and the state estimated by the particle filter may never converge. On the other 60 hand, some constraining schemes impose constraints on all particles (instead of the state estimate) and thus equivalently sample particles from a constrained proposal density function [30, 34, 35]. We refer to the approaches, which impose the constraints on all particles, as *point-wise density truncation* (PruDENT) 65 [36]. When constraints are enforced on the estimate, e.g., the statistical expectation or the mean of the state, as is the case with the synergy activation coefficients, a particle filter with PruDENT (PF-PruDENT) may lead to more stringent conditions than actually desired and may also result in possibly irrelevant conditions [37].

We introduce a new constrained state estimation algorithm for particle filters referred to as the *mean density truncation* (MiND). MiND relies on the principle of minimal perturbation of the (unconstrained) state density function 70 to satisfy the desired constraints. Specifically, we impose the constraint on the mean of the unknown state by perturbing the unconstrained posterior density using only one particle. We subsequently construct a sequence of probability 75 density functions that satisfy the constraint on the mean and converge to the unconstrained density in the norm sense.

The novelty of this paper include: 1) formulation of the movement identification problem in prosthesis control as a nonlinear state-space model using a physiologically relevant system dynamics and observation models; 2) derivation 80 of an optimal constrained particle filter algorithm, PF-MiND, for tracking synergy activation coefficients; and 3) prediction of hand and wrist movements using EMG data recorded from forearm muscles.

In Section 2, we outline the nonlinear state-space model the estimation of muscle synergies activation coefficients. Section 3 reviews the classical particle 85 filtering framework and introduces MiND, an optimal particle filter for constraints imposed on the mean of the state. In Section 4, we describe EMG data collection experiments for testing MiND. We present our results in Section 5 and discuss these results in Section 6. Lastly, we conclude in Section 7.

2. Mathematical Modeling

90 2.1. State-Space Model

The nonlinear state transitions in the CNS that are responsible for task-specific muscle activations are modeled using a sigmoid function, a special case of the Logistic function, of the form [26, 38]:

$$x_{n+1} = \frac{x_n}{\sqrt{1 + x_n^2}} + u_n, \quad (1)$$

where $x_n \in \mathbb{R}^k$ represents the unknown latent system state at time n and u_n zero-mean state noise sequence with known covariance matrix Q_n . The latent system state consists of nonnegative synergy activation coefficients $x_n = [x_{1,n}, \dots, x_{k,n}]^t$, where k is the total number of muscle synergies and t denotes matrix transpose operation.

95 The system measurement model is a linear mapping and is defined using the hypothesis of muscle synergies:

$$y_n = Wx_n + v_n, \quad (2)$$

where $y_n \in \mathbb{R}^m$ is the measurement vector, i.e., the vector of EMG signals, W is the muscle synergy matrix, v_n is a zero-mean measurement noise sequence with known covariance matrix R_n , and m is the total number of muscles or the number of EMG channels.

In addition, for neurological reasons that will be elaborated on in the sequel, the mean of the unknown latent system state x_n is constrained to be nonnegative:

$$E[x_n] \geq 0, \quad \forall n. \quad (3)$$

100 A schematic layout of the proposed mathematical model is presented in Fig. 1. The latent system state x_n consists of k muscle synergy activation coefficients and evolve nonlinearly over time n . The state x_n is related to the system output, i.e., the EMG signals y_n , through the muscle synergy matrix W . Given the surface EMG signals y_n recorded from forearm muscles, we aim to track the nonlinear latent system state x_n under the non-negativity constraint. The estimated coefficients x_n will be used to identify hand and wrist movements [17].

2.2. Muscle Synergies

Muscle synergies are hypothesized as fixed relative activation levels of different muscles that enable the recruitment of a large number of muscles by a small number of commands from the CNS [19, 20]. These commands are translated into individual muscle activations by a linear transformation, called the muscle synergy matrix W [39]. A schematic description of the hypothesis of muscle synergies is provided in Fig. 1. Mathematically

$$Y = W \times X, \quad (4)$$

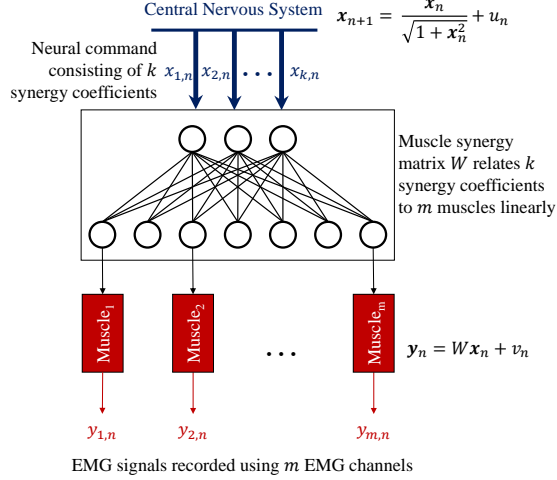


Figure 1: The proposed mathematical model for tracking synergy activation coefficients \mathbf{x}_n and identifying movements from EMG signals. The CNS is hypothesized to use a small set of synergy activation coefficients $\mathbf{x}_n = [x_{1,n}, \dots, x_{k,n}]^t$ to control a large set of m muscles through the muscle synergy matrix W ($m > k$). The latent system state \mathbf{x}_n consists of synergy activation coefficients and evolve nonlinearly over time. The system measurement model relates the system output, the EMG signals \mathbf{y}_n , to the synergy activation coefficients \mathbf{x}_n through the muscle synergy matrix W .

where $Y \in \mathbb{R}^{m \times T}$ represents the EMG data, $W \in \mathbb{R}^{m \times k}$ the synergy matrix,
110 $X \in \mathbb{R}^{k \times T}$ the matrix of synergy activation coefficients, and T is the total
number of time points of the EMG data recorded from forearm muscles. Due to
non-stationarity, and just like in speech processing, the EMG data is first divided
into analysis windows (e.g., 250 ms each). The root mean square (RMS) values
for each window and each channel are calculated separately.

115 In Eq. 4, Y , i.e., the matrix of the processed EMG data is known while both
 W and X are unknown. Thus, the identification of muscle synergies W and
synergy activation coefficients X amounts to a blind source separation (BSS)
problem. In the literature, various BSS algorithms have been proposed for esti-
120 mation of the muscle synergy matrix W , including principal component analysis
(PCA), independent component analysis (ICA), probabilistic ICA (pICA) and
nonnegative matrix factorization (NMF) [22, 39, 40]. In an earlier work, Rasool
et al. compared the performance of two popular algorithms for muscle synergy
extraction, i.e., pICA and NMF [17]. They found that pICA algorithm per-
formed better albeit at a slightly higher computational cost [17]. We also found
125 that pICA performed better than NMF for our application. Please refer to Fig.
4 A.

2.3. Non-Negativity Constraint

The muscle synergy activation coefficients quantify the contribution of each synergy towards the muscle activation during performance of a task. Therefore,

130 these coefficients are constrained to be nonnegative. Physiologically, starting from the motor cortex in the brain to the spinal cord and finally to the skeletal muscles, there are numerous excitatory, inhibitory, and reflex circuits consisting of motor neurons, interneurons, Renshaw cells, and sensory organs, i.e., Golgi tendon organs and muscle spindles [38, 41]. The internal state of these circuits
 135 can have any real number, positive or negative, because of the possible excitatory as well as inhibitory inputs [38]. However, the expected value of the state will always be nonnegative, i.e., the synergy activation coefficient will be zero when the corresponding muscle synergy is not contributing and positive when the synergy is contributing to the activation of muscles. Therefore, we must
 140 constrain the mean of the unknown state: $E[\mathbf{x}_n] \geq 0$ for all time instants $n = 1, 2, \dots, T$.

3. Constrained Particle Filtering

3.1. Bayesian Recursion

In the Bayesian framework, the optimal inference of the state \mathbf{x}_n using the observation history $\mathbf{y}_{1:n} = [\mathbf{y}_1, \dots, \mathbf{y}_n]$ relies on the posterior density $p(\mathbf{x}_n | \mathbf{y}_{1:n})$. The optimal minimum mean square error estimate of \mathbf{x}_n is given by the expected value of the posterior density, i.e., $\mathbb{E}(\mathbf{x}_n | \mathbf{y}_{1:n})$. Using Bayes' rule, the posterior density can be computed recursively:

$$p(\mathbf{x}_n | \mathbf{y}_{1:n-1}) = \int p(\mathbf{x}_{n-1} | \mathbf{y}_{1:n-1}) p(\mathbf{x}_n | \mathbf{x}_{n-1}) d\mathbf{x}_{n-1}, \quad (5)$$

$$p(\mathbf{x}_n | \mathbf{y}_{1:n}) = \frac{p(\mathbf{y}_n | \mathbf{x}_n) p(\mathbf{x}_n | \mathbf{y}_{1:n-1})}{\int p(\mathbf{y}_n | \mathbf{x}_n) p(\mathbf{x}_n | \mathbf{y}_{1:n-1}) d\mathbf{x}_n}. \quad (6)$$

However, in the nonlinear case (5) and (6) are only a conceptual solution as
 145 the integral in the denominator of (6) is, in general, intractable.

3.2. Particle Filters

Particle filters approximate the posterior density of the unknown state using a set of N particles and their associated weights $\{\mathbf{x}_n^{(i)}, w_n^{(i)}\}_{i=1}^N$:

$$p^N(\mathbf{x}_n | \mathbf{y}_{1:n}) = \sum_{i=1}^N w_n^{(i)} \delta(\mathbf{x}_n - \mathbf{x}_n^{(i)}), \quad (7)$$

where δ is the Dirac delta function. Ideally, the particles should be sampled from the true posterior density, which is unknown. Therefore, a *proposal density* or an *importance distribution* $q(\mathbf{x}_n | \mathbf{x}_{n-1}, \mathbf{y}_n)$ is used instead [27, 42]. To make up the difference between the importance and posterior distributions, the particles are weighted as follows:

$$\tilde{w}_n^{(i)} = w_{n-1}^{(i)} \frac{p(\mathbf{y}_n | \mathbf{x}_n^{(i)}) p(\mathbf{x}_n^{(i)} | \mathbf{x}_{n-1}^{(i)})}{q(\mathbf{x}_n^{(i)} | \mathbf{x}_{n-1}^{(i)}, \mathbf{y}_n)}. \quad (8)$$

The normalized weight of particle i at time n is given by:

$$w_n^{(i)} = \frac{\tilde{w}_n^{(i)}}{\sum_{j=1}^N \tilde{w}_n^{(j)}}. \quad (9)$$

The conditional mean estimate of the state is then given by:

$$\hat{\mathbf{x}}_n = \mathbb{E}[\mathbf{x}_n | \mathbf{y}_{1:n}] \approx \sum_{i=1}^N w_n^{(i)} \mathbf{x}_n^{(i)}. \quad (10)$$

The particle filter is shown to converge to the true posterior distribution when the number of particles increases [27]. The variance of state estimate by the particle filter may increase exponentially with time and is generally addressed using *re-sampling* [27]. A popular re-sampling algorithm, referred to as systematic re-sampling, selects particles according to their weights and assigns equal weights $\frac{1}{N}$ to all selected N particles [27].

Systematic Re-sampling: Sample $U_1 \sim \mathcal{U}[0, \frac{1}{N}]$ and define $U_i = U_1 + \frac{i-1}{N}$ for $i = 2, \dots, N$, then set $N_n^{(i)} = |\{U_j : \sum_{k=1}^{i-1} w_n^{(k)} \leq U_j \leq \sum_{k=1}^i w_n^{(k)}\}|$ with the convention $\sum_{k=1}^0 := 0$.

3.3. Constrained Particle Filters

We consider the constrained discrete state-space model given in (1) and (2) and subject to additional constraint on the mean of the state:

$$a_n \leq \phi_n(\hat{\mathbf{x}}_n) \leq b_n, \quad (11)$$

where ϕ_n represents the constraint function at time n . Note that the constraint should only be satisfied by the state estimate provided by the conditional mean as defined:

$$\phi_n(\hat{\mathbf{x}}_n) = \phi_n(\mathbb{E}[\mathbf{x}_n | \mathbf{y}_{1:n}]) \approx \phi_n \left(\sum_{i=1}^N w_n^{(i)} \mathbf{x}_n^{(i)} \right). \quad (12)$$

In the sequel and without loss of generality, we consider ϕ_n to be the identity function for all n , i.e., the interval-constraint is applied to the conditional mean rather than a function of the mean.

3.4. Pointwise Density Truncation (PruDENT)

Current approaches for constrained state estimation in particle filters enforce constraints on all particles [29, 32, 33]. Fundamentally, constraining every particle to the interval $[a_n, b_n]$ is equivalent to constraining the support of the posterior density $p(\mathbf{x}_n | \mathbf{y}_{1:n})$ to this interval. However, when the constraint is imposed on the conditional mean only, then constraining the entire density is irrelevant and can lead to erroneous estimates. In particular, the point-wise density truncation (PruDENT) approach will always result in large estimation errors unless the unconstrained density had a bounded support [43]. PruDENT will result in bounded estimation errors only when the unconstrained posterior density is already inside the constraining interval [43].

3.5. Mean Density Truncation (MiND)

We propose a minimal perturbation strategy such that the constrained posterior density is “close” to the unconstrained posterior density. Our strategy relies on constraining one particle (rather than all particles) to satisfy the interval constraint $a_n \leq \phi_n(\hat{\mathbf{x}}_n) \leq b_n$. We start by generating N unconstrained particles from the proposal distribution $q(\mathbf{x}_n | \mathbf{x}_{n-1}, \mathbf{y}_n)$ following the framework of conventional particle filters. If the conditional mean estimate \hat{x}_n , using this N -order approximation, satisfies the constraint, then we retain these particles. Otherwise, we remove the particle located furthest from the boundary of the feasible region, i.e., the constraining interval $[a_n, b_n]$ and replace it with another particle that is drawn from the high probability region. This process of removing/adding one particle can be viewed as a “minimal perturbation” of the unconstrained density using only one particle.

For simplicity and without loss of generality, we assume that the particle weights are given by the likelihood function $p(\mathbf{y}_n | \mathbf{x}_n)$, i.e., the proposal density $q(\mathbf{x}_n | \mathbf{x}_{n-1}, \mathbf{y}_n)$ is the transition distribution function $p(\mathbf{x}_n | \mathbf{x}_{n-1})$.

Consider a time step n after re-sampling, all particles have the same weight $w_n^{(i)} = \frac{1}{N}$, for all $1 \leq i \leq N$. We remove a particle that is furthest from the constrained region and add another particle $(x_n^{(N)}, \frac{1}{N})$ that enforces the constraint on the mean estimate as follows:

$$a_n \leq \frac{1}{N} \sum_{i=1}^{N-1} x_n^{(i)} + \frac{1}{N} x_n^{(N)} \leq b_n, \quad (13)$$

$$a'_n \leq x_n^{(N)} \leq b'_n, \quad (14)$$

where $a'_n = Na_n - \sum_{i=1}^{N-1} x_n^{(i)}$ and $b'_n = Nb_n - \sum_{i=1}^{N-1} x_n^{(i)}$. The detailed steps of PF-MiND are presented in algorithm 1.

3.6. On the Convergence of MiND

Let (Ω, \mathcal{F}, P) be a probability space where the stochastic processes $\{\mathbf{x}_n, n \in \mathbb{N}\}$ and $\{\mathbf{y}_n, n \in \mathbb{N}\}$ are defined. Let $\mathcal{B}(\mathbb{R}^n)$ be the Borel σ -algebra on \mathbb{R}^n . If μ is a signed measure, then the full variation of μ , $|\mu|$, is defined by

$$|\mu|(\Omega) = \sup_{A \in \mathcal{B}, A \subset \Omega} (|\mu(A)| + |\mu(\Omega \setminus A)|). \quad (15)$$

Theorem 1. Let p^N be the discrete approximation of the posterior density function of the unconstrained system, and p_{MiND}^N be the discrete approximation of the density underlying the MiND algorithm. We have

$$\lim_{N \rightarrow \infty} |p^N - p_{\text{MiND}}^N| = 0, \quad (16)$$

where $|\mu|$ denotes the full variation of the measure μ .

Algorithm 1 Particle Filtering with Mean Density Truncation (PF-MiND)

Initialization

Define $C_n = \{\boldsymbol{x}_n : a_n \leq \hat{x}_n \leq b_n\}$.

for $j = 1, 2, \dots, N$ **do**

 Generate $x_0^{(j)} \sim \mathcal{N}(\boldsymbol{x}_0^{(j)}, R_n)$.

 Compute the initial weights using (8) and normalize.

end for

for $n = 1, 2, \dots, T$ **do**

Unconstrained estimation

for $j = 1, 2, \dots, N$ **do**

 Generate sample $x_n^{(j)}$ from the system dynamics model (1).

 Compute weight using: $\tilde{w}_n^{(j)} = \tilde{w}_{n-1}^{(j)} p(\boldsymbol{y}_n | \boldsymbol{x}_n^{(j)})$.

end for

Normalize particle weights $w_n^{(i)} = \tilde{w}_n^{(i)} / \sum_{j=1}^N \tilde{w}_n^{(j)}$.

Resample $\{x_n^{(i)}, \frac{1}{N}\}_{i=1}^N$.

Compute the weighted mean $\hat{\boldsymbol{x}}_n = \sum_{i=1}^N \frac{1}{N} x_n^{(i)}$.

Constrained estimation

if $\hat{\boldsymbol{x}}_n \notin C_n$ **then**

 Remove the furthest particle $x_n^{(i)}$.

 Add a new particle x_n^N using Eqs. (13)-(14).

 Compute the constrained weighted mean $\hat{\boldsymbol{x}}_n = \sum_{i=1}^N \frac{1}{N} \boldsymbol{x}_n^{(i)}$.

end if

end for

Proof. By construction, we have

$$p_{\text{MiND}}^N = p^N \left(1 - \frac{1}{N}\right) + \frac{1}{N} \delta(\boldsymbol{x} - \boldsymbol{x}^N). \quad (17)$$

Hence,

$$|p_{\text{MiND}}^N - p^N| = \left| -\frac{1}{N} p^N + \frac{1}{N} \delta(\boldsymbol{x} - \boldsymbol{x}^N) \right| \quad (18)$$

$$\leq \frac{1}{N} |p^N| + \frac{1}{N} |\delta(\boldsymbol{x} - \boldsymbol{x}^N)| \quad (19)$$

$$= \frac{2}{N}, \quad (20)$$

because $|p^N| = |\delta(\boldsymbol{x} - \boldsymbol{x}^N)| = 1$. Thus, $\lim_{N \rightarrow \infty} |p_{\text{MiND}}^N - p^N| \leq \lim_{N \rightarrow \infty} \frac{2}{N} = 0$. \square

It is important to clarify that although the density estimated by MiND converges to the unconstrained density in the variation norm, it does not mean

that the unconstrained density satisfies the constraint. This is because the convergence of densities does not imply convergence of their means. In fact,
200 the expectation operator is linear, but not continuous. When the support of densities is infinite, the convergence of zero moments (densities) does not imply convergence of the first moments (expectations).

4. Methods

4.1. EMG Data Recording

205 A total of twelve able-bodied individuals (four females and eight males) volunteered for the study. The mean age of the participants was 28.2 years with single standard deviation of 6 and half years. All participants were healthy, right hand dominant with no neuromuscular disorder history. An institutional review board approved the experimental protocol. An informed consent was signed by
210 all participants before the start of the experiment. We selected two types of hand and wrist movements, i.e., single degree-of-freedom (1-DOF) and 2-DOF. The first set consisted of six 1-DOF hand and wrist movements including hand open, hand close, wrist flexion, wrist extension, forearm pronation, and forearm supination. The second set consisted of eighteen movements and included all
215 six 1-DOF movements as well as their possible combinations. Both sets of movements, i.e., 1-DOF and (1+2)-DOF are described in Table 1. We also included ‘rest’ (RT) or ‘no movement’ in each set.

Table 1: Description of 1-DOF (6 in total) and 2-DOF (12 in total) hand and wrist movements

1-DOF Movements	2-DOF Movements	
Hand Open (HO)	HO + WF	HC + FP
Hand Close (HC)	HO + WE	HC + FS
Wrist Flexion (WF)	HO + FP	WF + FP
Wrist Extension (WE)	HO + FS	WF + FS
Forearm Pronation (FP)	HC + WF	WE + FP
Forearm Supination (FS)	HC + WE	WE + FS

At the start of the experiment the participants were seated comfortably in a chair with elbow flexed at 90° and arm abducted at 10°. A graphical user interface (GUI) was used to provide visual and auditory cues to the participant for guiding through the data collection process [44]. A single trial consisted of four repetitions of each movement and each repetition was five seconds long.
220 There was a short break of five seconds between consecutive repetitions. Participants were instructed to maintain comfortable and repeatable force levels for all movements.
225

The EMG data were recorded from eight forearm muscles using disposable, Ag/AgCl snap electrodes with two circular conductive areas of 1 cm each and an inter-electrode distance of 2 cm. All electrodes were placed around the circumference of the forearm symmetrically. The electrodes were placed at the proximal end of the forearm at a location of 1/3 of the distance between medial
230

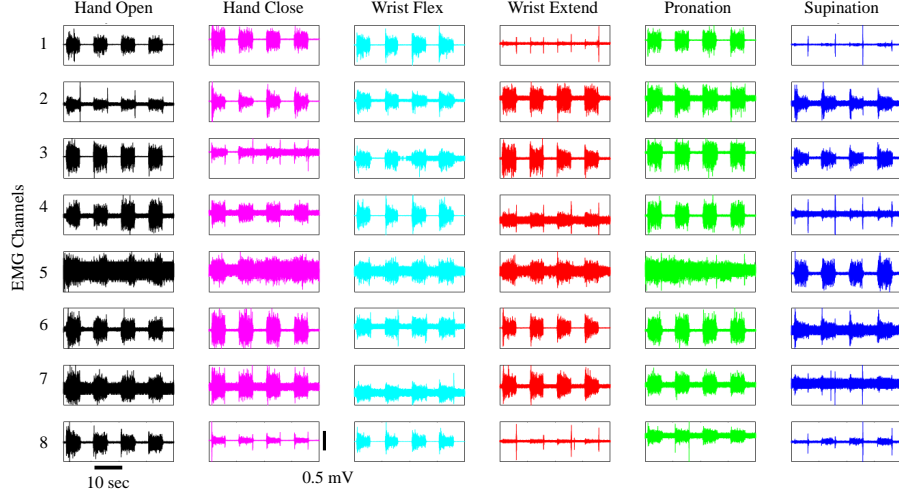


Figure 2: Raw EMG signals from a representative participant. Each column represents one of the six 1-DOF movements indicated on the top. Each row represents an EMG channel as indicated on the left. We note four active regions in each plot that show EMG envelopes for four trials of each movement. Low amplitude EMG signals represent rest period between two trials. We note sudden spikes in some EMG channels towards the end of a trial which are possibly related to movement artifacts.

epicondyle of the humerus and styloid process of the ulna. A Noraxon (Noraxon U.S.A. Inc, Scottsdale, Arizona) TeleMyo Direct Transmission System was used to record the EMG data at the sampling rate of 1500 Hz.

4.2. EMG Data Processing

The EMG data were partitioned using non-overlapping analysis windows of size 250 ms each and RMS values for each channel were calculated in all analysis windows. This resulted in the measurement matrix $Y = [y_1, y_2, \dots, y_T]$ with $y_n = [y_{1,n}, y_{2,n}, \dots, y_{m,n}]^t$, where $y_{m,n}$ represents RMS EMG data from muscle m at time n . Raw EMG data from all eight EMG channels and six 1-DOF movements of a representative participant are shown in Fig. 2

4.3. Movement Identification Algorithm

Our proposed algorithm consisted of two parts or modes: 1) training mode included extraction of muscle synergies; and 2) testing mode included estimation of synergy activation coefficients (i.e., the system state) and subsequently using these for identification of hand and wrist movements. A schematic layout of the algorithm is presented in Fig. 3. The EMG data from all trials were randomly divided into two parts, training and testing. Muscle synergies were extracted using training data (75% of total data) and movement identification was performed using testing data (remaining 25% of total data).

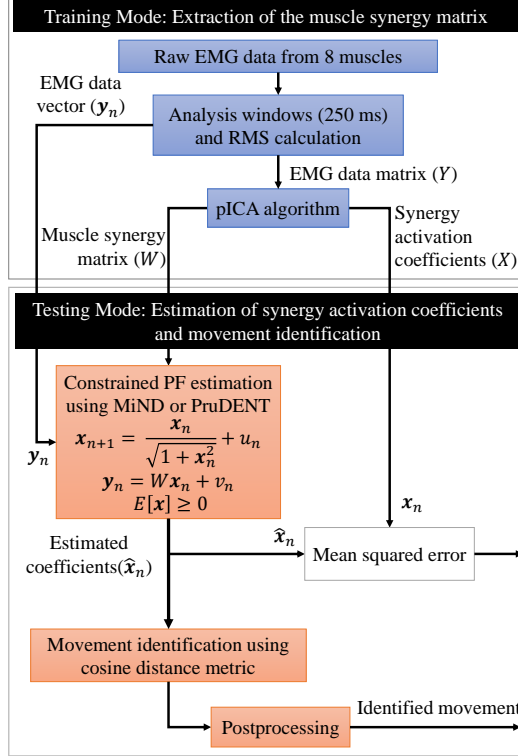


Figure 3: A schematic layout of the proposed algorithm for the identification of hand and wrist movements using state-space model and muscle synergies. The input of the proposed algorithm consists of multichannel EMG signals and the output is the identified movement. The proposed algorithm consists of two parts/modes, i.e., training and testing. In the training mode, we extract muscle synergies and in the testing mode, we first estimate synergy activation coefficients using constrained particle filter and later identify performed movement. The testing mode can run in both off-line as well as online settings.

²⁵⁰ 4.3.1. Extraction of Muscle Synergies (Training Mode)

The muscle synergy matrix W and corresponding activation coefficients X can be extracted from RMS EMG data Y using BSS algorithms. The synergy activation coefficients X were considered ground truth and were used later to evaluate the performance and benchmark proposed algorithm. It is important ²⁵⁵ to note that these coefficients were not required for movement identification in the testing mode. The computational time for the extraction of muscle synergies using pICA algorithm was 4.69 milliseconds (ms) as compared to 0.14 ms for the NMF algorithm.

The variance accounted for (VAF) is a commonly used metric to determine ²⁶⁰ the number of synergies (independent components) required to represent the data effectively in a low dimensional subspace [17, 45]. We selected the least number of synergies that accounted for 99% of the variance of recorded EMG

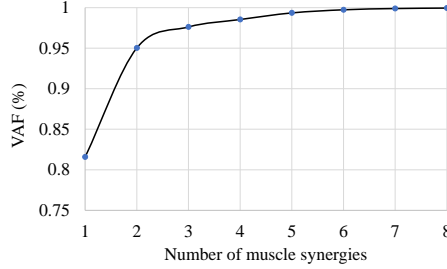


Figure 4: Variance Accounted For (VAF) is presented for a representative participant as a function of the number of extracted muscle synergies. We found that the least number of synergies required for 99% VAF was four.

265 data. In Figure 4(B), we present the effect of increasing the number of synergies
 on VAF for (1+2)-DOF movements of a representative participant. We found
 that four muscle synergies were sufficient to capture 99% VAF, i.e., the state
 vector would consist of four components $\mathbf{x}_n = [x_{1,n}, \dots, x_{4,n}]^t$.

4.3.2. Estimation (Tracking) of the Synergy Activation Coefficients (Testing Mode)

270 In the testing mode, particle filters with both state constraining algorithms,
 i.e., PruDENT and MiND were used to track synergy activation coefficients
 $\hat{\mathbf{x}}_n = [\hat{x}_{1,n}, \dots, \hat{x}_{4,n}]^t$ given the measurement vector, i.e., the EMG data \mathbf{y}_n .
 We used 5000 particles for each estimation and performed 100 Monte Carlo runs.
 It is important to highlight that Monte Carlo runs were performed to benchmark
 the algorithm and no Monte Carlo simulations are required for real-time/off-line
 275 movement identification.

4.3.3. Wrist and Hand Movement Identification (Testing Mode)

280 We used the estimated synergy activation coefficients $\hat{\mathbf{x}}_n$ to identify the per-
 formed hand and wrist movements with the cosine distance metric [17]. Finally,
 post-processing was performed to further improve movement identification de-
 cisions. Details of the post-processing algorithm are provided in Ref. [17]. The
 identification error data presented in the Results Section were averaged over all
 Monte Carlo runs and all 1-DOF or (1+2)-DOF movements. We compared the
 285 performance of the proposed PF-MiND algorithm to PF-PruDENT and to lin-
 ear discriminant analysis (LDA), one of the best performing algorithm in EMG
 prosthesis control literature [12, 13, 46]. We used four most commonly used
 features for the LDA including mean absolute value, zero crossing, slope sign
 change and waveform length [17].

The steps for movement identification are summarized below:

Step 1: Divide RMS EMG data into S task-specific bins, i.e., Y^s , where $s =$
 290 $1, \dots, S$, and S is the total number of movements.

Step 2: Partition each Y^s into training and testing datasets.

- Step 3: Extract muscle synergy matrices W^s using the training dataset; one for each movement.
- Step 4: Run S constrained particle filters on test dataset and estimate $\hat{\mathbf{x}}_n$.
- ²⁹⁵ Step 5: Reconstruct muscle activations using: $\hat{y}_n^s = W^s \hat{\mathbf{x}}_n^s$.
- Step 6: Calculate cosine distance between estimated and actual muscle activation using: $d_n^s = \text{Cosine}[\hat{y}_n^s, y_n]$.
- Step 7: Identify movement n using: $I_n = \text{Min}[d_n^1, \dots, d_n^S]$.
- ³⁰⁰ Step 8: Perform post-processing using posterior probabilities of the LDA algorithm and the cosine distance d_n^s calculated above [17].

4.4. Robustness Analysis

We analyzed the robustness of both MiND and PruDENT algorithms by adding synthetic white (zero-mean) Gaussian noise to the recorded EMG data. The signal to noise ratio (SNR) was used to measure the level of EMG signal to the level of the noise using:

$$\text{SNR} = 10 \log_{10} \frac{P_{\text{EMG}}}{P_{\text{Noise}}}, \quad (21)$$

where P represents the power of the signal. The SNR of the recorded EMG signal was considered as the baseline and both state constraining schemes (PruDENT and MiND) were tested for a range of SNR values, $\text{SNR} = [-10, -5, 0, 1, 5, 10, 20]$.
³⁰⁵

4.5. Statistical Analysis

The movement identification errors from both state constraining schemes, i.e., PruDENT and MiND and from LDA algorithm were tested for normality (Gaussian distribution) using the Kolmogorov-Smirnov test, where the null hypothesis was that the standardized data follows a Gaussian distribution. We were unable to reject the null hypothesis at 95% significance ($p > 0.05$). Therefore the identification errors from all algorithms were compared using the Student's t-test with probability of type-I error $\alpha = 0.05$.
³¹⁰

The mean squared errors, calculated between the actual and estimated synergy activation coefficients, were also tested for normality using the Kolmogorov-Smirnov test. The null hypothesis was rejected at 95% significance ($p < 0.001$). Therefore, for this dataset the statistical analyses was performed using non-parametric statistics (Wilcoxon signed-rank test) with probability of type-I error $\alpha = 0.05$ and p values with Z scores were presented.
³¹⁵

320 **5. Results**

5.1. Synergy Activation Coefficients

We tracked state vector that consisted of four synergy activation coefficients using PF-PruDENT and PF-MiND. The tracking results for all four state coefficients x_1, \dots, x_4 are presented in Fig. 5(a). The cumulative absolute errors given by $\sum |x_k - \hat{x}_k|$ for both PF-PruDENT and PF-MiND are shown in Fig. 325 5(a).

In Fig. 5(b), we present mean squared errors of both PF-PruDENT and PF-MiND for all four state coefficients. Cumulative mean squared errors $\sum \text{MSE}_k$ for each state are also shown. We observed significantly lower estimation errors for the PF-MiND as compared to PruDENT for all four state coefficients. A Wilcoxon signed-rank test showed that the differences between mean squared errors of PF-PruDENT and PF-MiND were statistically significant for all four state coefficients. The Z and p values for the synergy activation coefficients are as follows: $x_1: Z = -11.24, p < 0.001$, $x_2: Z = -13.77, p < 0.001$, $x_3: Z = -13.29, p < 0.001$, $x_4: Z = -13.16, p < 0.001$, and for the pooled mean 330 335 squared error data from all four synergy coefficients: $Z = -25.25, p < 0.001$.

In Fig. 6, we demonstrate the performance of the proposed PF-MiND for different number of particles; i.e., mean squared tracking error in the state estimation as a function of number of particles. It is evident that the state 340 estimation mean squared error decreases as the number of particle increase.

5.2. Robustness Assessment

For robustness testing, the SNR of the EMG data was changed by adding white Gaussian noise before estimation of synergy activation coefficients. The robustness results are presented in Fig. 7. Each sub-figure represents a synergy 345 350 activation coefficient with mean squared error in the y-axis and the SNR in the x-axis. We observed that PF-MiND performed robustly as compared to PF-PruDENT especially at low SNR values across all four synergy activation coefficients. A Wilcoxon signed-rank test showed that, at all tested SNR values, the differences between mean squared errors of PF-PruDENT and PF-MiND were statistically significant ($p < 0.01$).

5.3. Movement Identification

The estimated synergy activation coefficients $(\hat{x}_1, \dots, \hat{x}_4)$ were later used to identify hand and wrist movements of all participants. The identified movements were compared with the ground truth (i.e., the actual movements performed by 355 participants) and movement identification errors were calculated. Movement identification errors for all twelve participants and for both sets of movements (1-DOF and 1+2 DOF) are presented in Fig. 8 using bar graphs. Each set of bars represents mean errors for a single participant and capped lines on top of each bar show single standard deviation. The classification errors for LDA, PF-PruDENT and PF-MiND are shown, respectively, in black, blue and red. The last set of bars represent mean values calculated across all tested 360 365 participants.

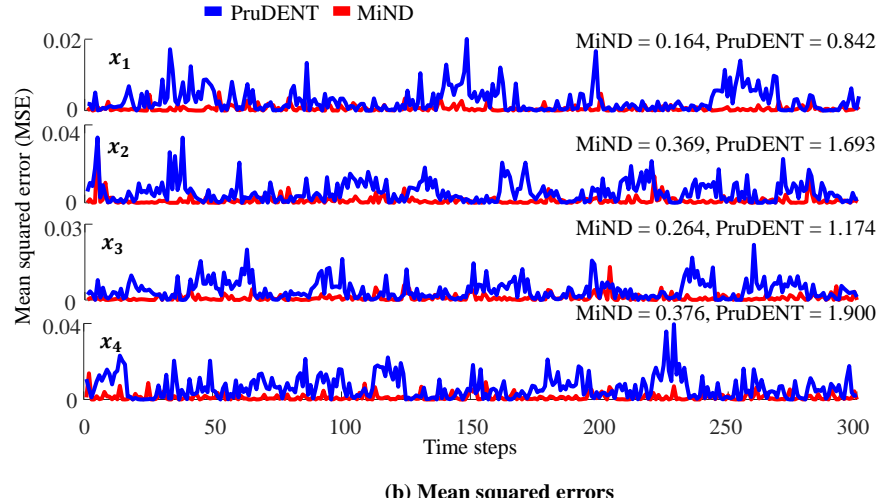
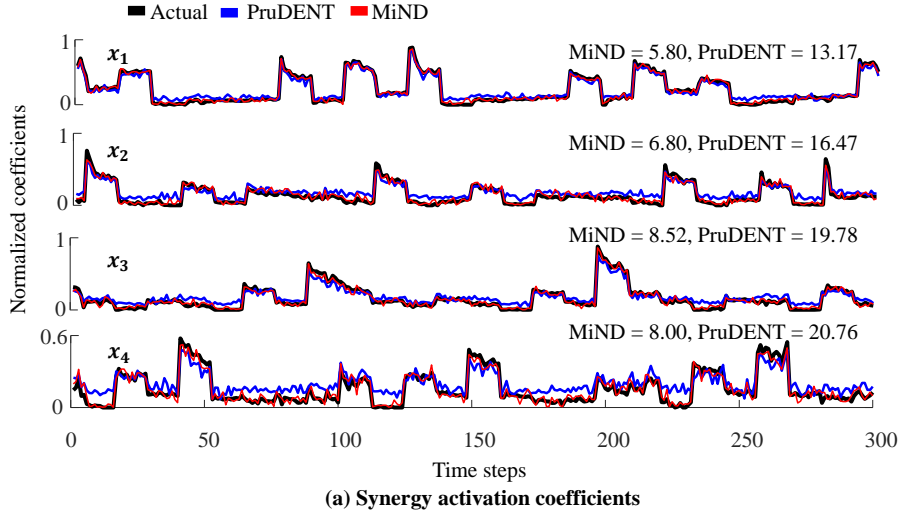


Figure 5: (a) Time history of four synergy coefficients (x_1, \dots, x_4) tracked using PF-PruDENT (blue), and PF-MiND (red). The black lines represent actual (ground truth) synergy activation coefficient data. The absolute cumulative error $\sum_{k=1}^{300} |x_k - \hat{x}_k|$ is also shown for each synergy activation coefficient. It is evident that PF-MiND was able to track all four synergy coefficients closely with small absolute cumulative error as compared to PF-PruDENT. (b) The mean squared errors between actual (x_1, \dots, x_4) and estimated states using PF-PruDENT (blue) and PF-MiND (red). The cumulative mean square errors given by $\sum_{k=1}^{300} \text{MSE}_k$ for both PF-PruDENT and PF-MiND are also shown for each state.

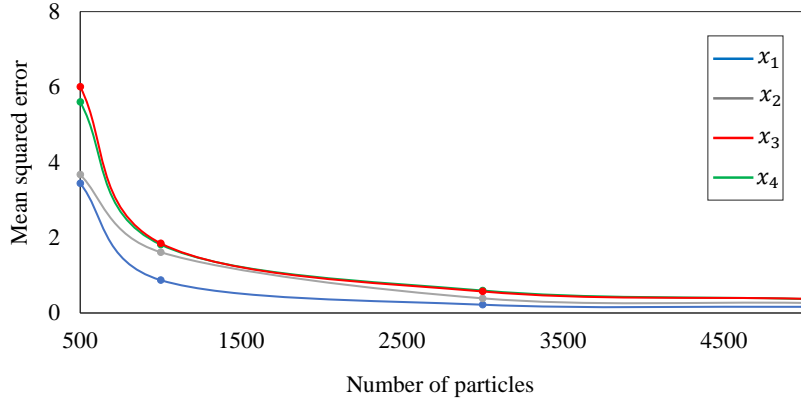


Figure 6: Mean squared tracking errors for four synergy activation coefficients (x_1, \dots, x_4) using PF-MiND for a range of number of particles.

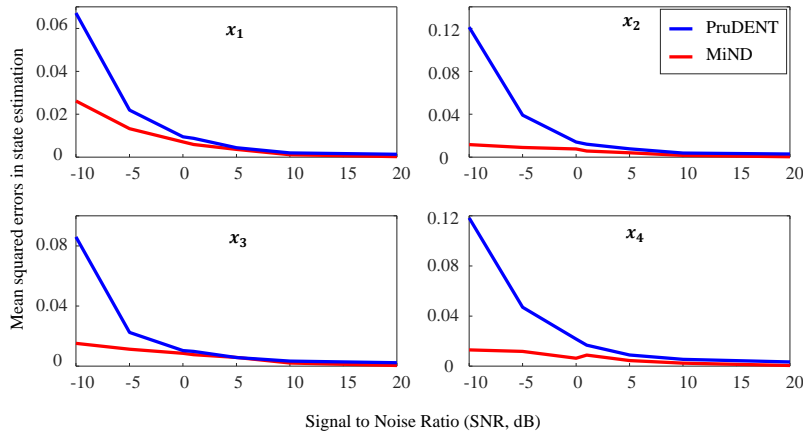


Figure 7: Mean squared errors in tracking four synergy activation coefficients (x_1, \dots, x_4), with PF-PruDENT and PF-MiND at different SNR values. The EMG data was corrupted synthetically using additive white Gaussian noise for a range of SNR values: SNR = [-10, -5, 0, 1, 5, 10, 20] dB. Statistical analyses performed using Wilcoxon signed-rank test showed that the differences between estimation errors of both PruDENT and MiND were statistically significant ($p < 0.01$).

participants. The stars (*) represent statistical significance ($p < 0.05$) between mean identification errors of PF-MiND with LDA and PF-PruDENT. For both sets of hand and wrist movements, the identification errors of PF-MiND were significantly lower than PF-PruDENT and LDA.

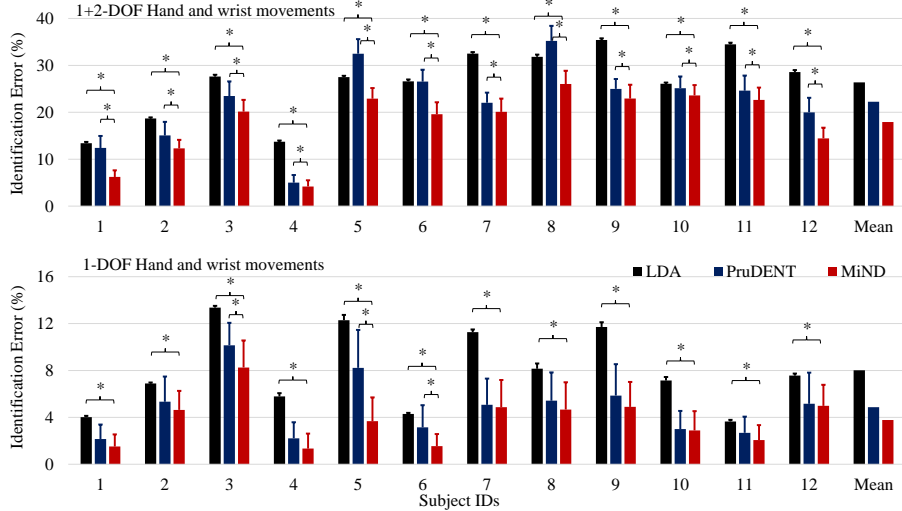


Figure 8: Mean movement identification errors of all twelve participants for the linear discriminant analysis LDA (black), PF-PruDENT (blue) and PF-MiND (red). The bars represent mean errors across all movements and the lines above the bars represent standard deviation for a single participant. The stars (*) represent statistical significance ($p < 0.05$). The last set of bars represents the mean values across all twelve participants. (Top) For (1+2)-DOF hand and wrist movements (19 in total including ‘rest’), PF-MiND performed better ($p < 0.05$) for all participants as compared to LDA and PF-PruDENT. (Bottom) For 1-DOF movements (7 in total including ‘rest’), PF-MiND performed better than LDA for all participants ($p < 0.05$). However, the differences between mean errors of PF-MiND and PF-PruDENT were not significant for some participants.

In Fig. 9, we present confusion matrices of a representative subject for three different algorithms; particle filtering with MiND (left), PruDENT (middle) and for the LDA (right). We noted that PF-MiND confused ‘hand close’ with ‘forearm pronation’, and ‘forearm pronation’ with ‘hand open’. The PF-PruDENT algorithm confused both ‘hand close’ and ‘forearm supination’ with ‘hand open’, and ‘wrist extension’ and ‘forearm supination’ with ‘rest’. LDA also confused various movements with each other except ‘rest’ and ‘wrist flexion’, which were correctly classified.

6. Discussion

We tackled the problem of identifying hand and wrist movements using non-negative synergy activation coefficients. We formulated a nonlinear state-space model and proposed a new algorithm for constrained state estimation using

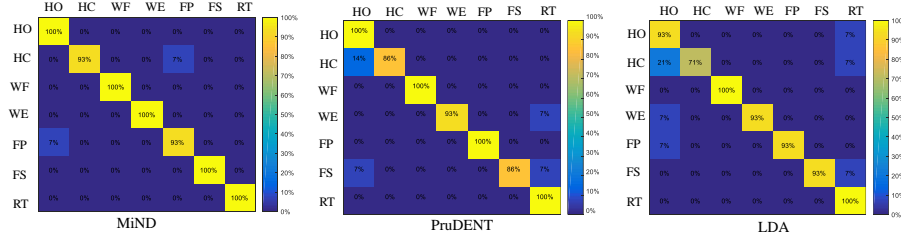


Figure 9: Confusion matrices for six movements and ‘rest’ are shown for PF-MiND (left), PF-PruDENT (middle) and LDA (right). Abbreviations used: HO - Hand Open, HC - Hand close, WF - Wrist Flexion, WE - Wrist Extension, FS - Forearm Supination, FP - Forearm Pronation, and RT - Rest.

particle filters. We established optimality properties of the constrained posterior distribution. We showed convergence to the unconstrained posterior, in line with the “minimum perturbation” principle of the algorithm. The proposed constrained particle filter was also robust under various noise conditions. The estimated synergy activation coefficients were used to identify 1-DOF and (1+2)-DOF hand and wrist movements of twelve participants with errors significantly lower than other contemporary approaches including the widely adopted LDA algorithm.

Previously, a linear system dynamics model was proposed and Kalman filter was used to estimate the constrained state [17, 18]. However, the complex processes that take place in the brain and spinal cord and govern the evolution of synergy activation coefficients lead to nonlinear dynamics [26]. The nonlinear behavior may also arise from neuronal transportation delays, firing saturation, and thresholding actions of individual interneurons and motor neurons. In particular, a simple linear process (random walk model [17, 18]) may not adequately capture the dynamics of the CNS. The assumption of linear dynamics may result in increased errors in movement identification as well as prosthesis control.

In this study, we used the sigmoid function to model nonlinear effect of saturation. The sigmoid function models linear growth and saturation in a physical system and is used extensively in artificial neural networks for smooth thresholding as well as signal clipping [47]. The neural processes taking place in the brain and spinal cord are very complex and modeling these with a sigmoid function may amount to gross simplification of the phenomenon [38]. However, modeling a set of neurons for input-output relation involves a trade-off between biological realism and computational efforts. It has been shown that the input-output relationship of corticospinal pathways of an intrinsic hand and leg muscles can be approximated using a sigmoid function [26]. The sigmoid functions has also been used to model a pool of interneurons and motor neurons in the spinal cord [38, 41]. Furthermore, the sigmoid function appears to be the first model of spinal cord circuitry to deal with the shifting patterns of synergistic and antagonistic muscle activity that necessarily accompany multi-muscle, multi-degree-of-freedom systems [38]. Finally, we believe we have chosen a simple

⁴¹⁰ function that model system dynamics as well as does not compromise accuracy of our system.

⁴¹⁵ A study by Farrel and Weir showed that the length of optimal delay was in the range of 100 – 175 ms for average users [48]. However, later on, a study by Smith et al. explicitly focused on the question of length of the analysis window size [49]. Authors showed that the optimal window size of 250 ms provided a right balance between the competing effects of classification error and controller delay (please refer to Figs. 2 and 3 in Ref [49]). Our recent study also showed similar findings (please see Figure 6b in Ref [17]).

⁴²⁰ We found that pICA algorithm performed significantly better in terms of movement identification error ($p < 0.05$) for all participants. The better performance of the pICA algorithm is possibly linked to its independent component assumption, i.e., assuming that observations (EMG signals) are generated from a set of statistically independent non-Gaussian sources via a linear instantaneous mixing process corrupted by additive Gaussian noise [50, 51]. The assumptions of pICA algorithm are largely satisfied in our case, i.e., EMG data are non-Gaussian and the estimated states, i.e., the time history of synergy activation coefficients are statistically independent of each other. The CNS may actually utilize the independence principle and employ a minimum number of independent components to control a large set of muscles. Thus, an algorithm that accounts for the independence may perform better as compared to other algorithms that do not explicitly capture component independence [40].

⁴²⁵ The computational time required for the extraction of muscle synergies using pICA algorithm was longer than that of NMF; however, we consider that the synergy extraction time in the range of 5 ms is not a limiting factor for real-time operation of the algorithm as muscle synergies are extracted at training time only. Once the synergy matrices are available, movement identification can be performed in real-time as well as off-line mode without running pICA algorithm.

⁴³⁵ Particle filter, a Bayesian estimation framework for nonlinear and non-Gaussian dynamical systems, converges asymptotically towards the optimal filter, in the mean square error sense, as the number of particles increase, i.e., $N \rightarrow \infty$ [28]. However, incorporation of constraints in particle filters is not straightforward and various heuristics are generally used, e.g., PruDENT, where every particle, rather than the conditional mean of the posterior density, is subject to constraint [43]. By minimally perturbing the unconstrained density, we were able to satisfy the constraint and establish convergence properties of MiND.

⁴⁴⁰ The surface EMG signal is a noisy signal [1]. Apart from the biological noise, the surface electrodes may record significant noise from different sources, including power lines, perspiration on the skin, and movement or removal of the electrode from muscle skin [1]. Therefore, we evaluated the performance of the proposed MiND algorithm under noisy conditions, with different SNRs (Fig. 7). We observed that the proposed PF-MiND algorithm performed significantly better than PF-PruDENT and was also able to successfully track the state (synergy activation coefficients) at significantly lower SNR values. PF-MiND with pICA performed better ($p < 0.03$) for two participants as compared to PF-MiND with NMF in movement identification for a set (1+2)-DOF movements.

Therefore, we used the pICA algorithm for every (1+2)-DOF movements for all participants to extract the muscle synergies from the processed EMG data. PF-MiND outperformed ($p < 0.05$) for all participants the widely used LDA in movement identification for 1-DOF as well as (1+2)-DOF movements. However, PF-MiND was able to discriminate hand tasks with high accuracy, i.e., small identification error, for 1-DOF compared to (1+2)-DOF movements. The improved performance of MiND under noisy conditions and increased complexity of the movement (from 7 1-DOF movements to 19 (1+2)-DOF movements) stems from its affinity to the underlying state-space model (minimal perturbation principle) and its convergence properties.

7. Conclusion

We addressed the problem of movement identification for forearm prosthetic control using the nonnegative synergy activation coefficients. We introduced a nonlinear function for system dynamics and proposed the hypothesis of muscle synergies as the system measurement model. We introduced a novel scheme for estimation of the unknown state in the nonlinearly constrained system and established its convergence properties. We used EMG data from forearm muscles and tracked synergy activation coefficients with both the widely adopted PruDENT approach and the proposed MiND for a range of hand and wrist movements. We showed that MiND had a higher tracking accuracy ($p < 0.001$) and was also robust to noise ($p < 0.01$). The estimated coefficients from MiND were used to identify hand and wrist movements with identification errors lower ($p < 0.05$) than the state-of-the-art in the literature.

Acknowledgment

This work was supported by the National Science Foundation under Grants NSF CCF-1527822 and NSF ACI-1429467.

References

- [1] R. Merletti, P. Parker, Electromyography: Physiology, Engineering, and Noninvasive Applications, Wiley-IEEE Press, 2004.
- [2] D. Farina, R. Merletti, R. M. Enoka, The extraction of neural strategies from the surface EMG, *Journal of Applied Physiology* 96 (4) (2004) 1486–1495.
- [3] D. Farina, R. Merletti, R. M. Enoka, The extraction of neural strategies from the surface EMG: an update, *Journal of Applied Physiology* 117 (11) (2014) 1215–1230.
- [4] C. De Luca, Electromyography, *Encyclopedia of Medical Devices and Instrumentation* (2006) 98–109.

- 495 [5] G. Rasool, B. Afsharipour, N. L. Suresh, W. Z. Rymer, Spatial analysis of multichannel surface EMG in hemiplegic stroke, *IEEE Transactions on Neural Systems and Rehabilitation Engineering* 25 (10) (2017) 1802–1811.
- 500 [6] M. Cifrek, V. Medved, S. Tonković, S. Ostojić, Surface EMG based muscle fatigue evaluation in biomechanics, *Clinical Biomechanics* 24 (4) (2009) 327–340.
- 505 [7] M. J. Zwarts, G. Drost, D. F. Stegeman, Recent progress in the diagnostic use of surface EMG for neurological diseases, *Journal of Electromyography and Kinesiology* 10 (5) (2000) 287–291.
- 510 [8] B. Afsharipour, M. Sandhu, G. Rasool, N. L. Suresh, W. Z. Rymer, Identifying spinal lesion site from surface EMG grid recordings, in: *Converging Clinical and Engineering Research on Neurorehabilitation II*, Vol. 15, Springer, 2017, pp. 39–43.
- 515 [9] A. L. Ciancio, F. Cordella, R. Barone, R. A. Romeo, A. D. Bellingegni, R. Sacchetti, A. Davalli, G. Di Pino, F. Ranieri, V. Di Lazzaro, E. Guglielmelli, L. Zollo, Control of prosthetic hands via the peripheral nervous system, *Frontiers in Neuroscience* 10 (2016) 116.
- 520 [10] D. Farina, N. Jiang, H. Rehbaum, A. Holobar, B. Graimann, H. Dietl, O. C. Aszmann, The extraction of neural information from the surface EMG for the control of upper-limb prostheses: emerging avenues and challenges, *IEEE Transactions on Neural Systems and Rehabilitation Engineering* 22 (4) (2014) 797–809.
- 525 [11] C. Castellini, P. van der Smagt, Surface EMG in advanced hand prosthetics, *Biological Cybernetics* 100 (1) (2009) 35–47.
- [12] S. Micera, J. Carpaneto, S. Raspovic, Control of hand prostheses using peripheral information, *IEEE Reviews in Biomedical Engineering* 3 (2010) 48–68.
- 530 [13] E. Scheme, K. Englehart, Electromyogram pattern recognition for control of powered upper-limb prostheses: State of the art and challenges for clinical use, *The Journal of Rehabilitation Research & Development* 48 (6) (2011) 643–660.
- 535 [14] F. Cordella, A. L. Ciancio, R. Sacchetti, A. Davalli, A. G. Cutti, E. Guglielmelli, L. Zollo, Literature review on needs of upper limb prosthesis users, *Frontiers in Neuroscience* 10 (2016) 209.
- 540 [15] N. Jiang, S. Dosen, K.-R. Muller, D. Farina, Myoelectric control of artificial limbs - is there a need to change focus?, *IEEE Signal Processing Magazine* 29 (5) (2012) 152 –150.

- 530 [16] B. Peerdeman, D. Boere, H. Witteveen, H. Hermens, S. Stramigioli, H. Rietman, P. Veltink, S. Misra, et al., Myoelectric forearm prostheses: state of the art from a user-centered perspective, *Journal of Rehabilitation Research & Development* 48 (6) (2011) 719–738.
- 535 [17] G. Rasool, K. Iqbal, N. Bouaynaya, G. White, Real-time task discrimination for myoelectric control employing task-specific muscle synergies, *IEEE Transactions on Neural Systems and Rehabilitation Engineering* 24 (1) (2016) 98–108.
- 540 [18] G. Rasool, K. Iqbal, N. Bouaynaya, G. White, Neural drive estimation using the hypothesis of muscle synergies and the state-constrained kalman filter, in: 2013 6th International IEEE/EMBS Conference on Neural Engineering (NER), San Diego, CA, USA, 2013.
- [19] E. Bizzi, V. Cheung, A. d'Avella, P. Saltiel, M. Tresch, Combining modules for movement, *Brain Research Reviews* 57 (1) (2008) 125–133.
- 545 [20] N. Jiang, H. Rehbaum, I. Vujaklija, B. Graimann, D. Farina, Intuitive, online, simultaneous, and proportional myoelectric control over two degrees-of-freedom in upper limb amputees, *IEEE Transactions on Neural Systems and Rehabilitation Engineering* 22 (3) (2014) 501–510.
- [21] M. C. Tresch, A. Jarc, The case for and against muscle synergies, *Current Opinion in Neurobiology* 19 (6) (2009) 601–607.
- 550 [22] G. K. Patel, C. Castellini, J. M. Hahne, D. Farina, S. Dosen, A classification method for myoelectric control of hand prostheses inspired by muscle coordination, *IEEE Transactions on Neural Systems and Rehabilitation Engineering* 26 (9) (2018) 1745–1755.
- 555 [23] E. Bizzi, V. C. Cheung, The neural origin of muscle synergies, *Frontiers in Computational Neuroscience* 7 (2013) 51.
- [24] M. Ison, P. Ardemiadis, The role of muscle synergies in myoelectric control: trends and challenges for simultaneous multifunction control, *Journal of Neural Engineering* 11 (5) (2014) 051001.
- 560 [25] T. Afzal, K. Iqbal, G. White, A. B. Wright, A method for locomotion mode identification using muscle synergies, *IEEE Transactions on Neural Systems and Rehabilitation Engineering* 25 (6) (2017) 608–617.
- [26] H. Devanne, B. A. Lavoie, C. Capaday, Input-output properties and gain changes in the human corticospinal pathway, *Experimental Brain Research* 114 (2) (1997) 329–338.
- 565 [27] A. Doucet, A. M. Johansen, *Handbook of Nonlinear Filtering*, Vol. 12, Oxford University Press, 2009, Ch. A tutorial on particle filtering and smoothing: Fifteen years later, pp. 656–704.

- [28] D. Crisan, A. Doucet, A survey of convergence results on particle filtering methods for practitioners, *IEEE Transaction on Signal Processing* 50 (3) (2002) 736–746.
- [29] L. Lang, W. S. Chen, B. R. Bakshi, P. K. Goel, S. Ungarala, Bayesian estimation via sequential monte carlo sampling constrained dynamic systems, *Automatica* 43 (9) (2007) 615–622.
- [30] X. Shao, B. Huang, J. M. Lee, Constrained bayesian state estimation: A comparative study and a new particle filter based approach, *Journal of Process Control* 20 (2) (2010) 143–157.
- [31] V. Pirard, E. Sviestins, A robust and efficient particle filter for target tracking with spatial constraints, in: International Conference on Information Fusion, Istanbul, Turkey, 2013.
- [32] Z. Zhao, B. Huang, F. Liu, Constrained Particle Filtering Methods for State Estimation of Nonlinear Process, Vol. 60, Wiley Online Library, 2014.
- [33] F. Papi, M. Podt, Y. Boers, G. Battistello, On constraints exploitation for particle filtering based target tracking, in: International Conference on Information Fusion, Singapore, 2012.
- [34] J. Prakash, S. C. Patwardhan, S. L. Shah, On the choice of importance distributions for unconstrained and constrained state estimation using particle filter, *Journal of Process Control* 21 (1) (2011) 3–16.
- [35] O. Straka, J. Dunik, M. Simandl, Truncation nonlinear filters for state estimation with nonlinear inequality constraints, *Automatica* 48 (2) (2012) 273–286.
- [36] N. Amor, N. Bouaynaya, P. Georgieva, R. Shterenberg, S. Chebbi, EEG dynamic source localization using constrained particle filtering, in: International Conference on Symposium Series on Computational Intelligence, Athens, Greece, 2016.
- [37] B. Ebinger, N. Bouaynaya, R. Polikar, R. Shterenberg, Constrained state estimation in particle filters, in: International Conference on Acoustics Speech and Signal Processing, Brisbane, Australia, 2015.
- [38] G. Raphael, G. A. Tsianos, G. E. Loeb, Spinal-like regulator facilitates control of a two-degree-of-freedom wrist, *Journal of Neuroscience* 30 (28) (2010) 9431–9444.
- [39] L. H. Ting, S. A. Chvatal, Decomposing muscle activity in motor tasks, in: Motor Control: Theories, Experiments, and Applications, Oxford University Press, 2010.
- [40] M. C. Tresch, V. C. Cheung, A. d'Avella, Matrix factorization algorithms for the identification of muscle synergies: Evaluation on simulated and experimental data sets, *Journal of Neurophysiology* 95 (4) (2006) 2199–2212.

- [41] T. Buhrmann, E. A. Di Paolo, Spinal circuits can accommodate interaction torques during multijoint limb movements, *Frontiers in Computational Neuroscience* 8 (2014) 144.
- 610 [42] N. Bouaynaya, D. Schonfeld, On the optimality of motion-based particle filtering, *IEEE Transactions on Circuits and Systems for Video Technology* 19 (7) (2009) 1068–1072.
- 615 [43] N. Amor, N. C. Bouaynaya, R. Shterenberg, S. Chebbi, On the convergence of the constrained particle filters, *IEEE Signal Processing Letter* 24 (6) (2017) 858–862.
- [44] M. Ortiz-Catalan, R. Branemark, B. Hakansson, Biopatrec: A modular research platform for the control of artificial limbs based on pattern recognition algorithms, *Source Code for Biology and Medicine* 8 (11) (2013) 1–18.
- 620 [45] G. Torres-Oviedo, J. M. Macpherson, L. H. Ting, Muscle synergy organization is robust across a variety of postural perturbations, *Journal of Neurophysiology* 96 (3) (2006) 1530–1546.
- 625 [46] M. A. Rahim, G. Rasool, N. Ahmad, EMG-controlled transradial prostheses—an investigation into machine learning techniques, *International Journal of Computer Applications* 174 (3) (2017) 1–8.
- [47] K. Gurney, An introduction to neural networks, CRC Press, 1997.
- [48] T. R. Farrell, R. F. Weir, The optimal controller delay for myoelectric prostheses, *IEEE Transactions on Neural Systems and Rehabilitation Engineering* 15 (1) (2007) 111–118.
- 630 [49] L. H. Smith, L. J. Hargrove, B. A. Lock, T. A. Kuiken, Determining the optimal window length for pattern recognition-based myoelectric control: Balancing the competing effects of classification error and controller delay, *IEEE Transactions on Neural Systems and Rehabilitation Engineering* 19 (2) (2011) 186–192.
- [50] P. Højen-Sørensen, O. Winther, L. Hansen, Mean-field approaches to independent component analysis, *Neural Computation* 14 (4) (2002) 889–918.
- 635 [51] C. Beckmann, S. Smith, Probabilistic independent component analysis for functional magnetic resonance imaging, *IEEE Transactions on Medical Imaging* 23 (2) (2004) 137–152.